


Article

Interconnected Micro, Meso, and Macro Porous Activated Carbon from Bacterial Nanocellulose for Superior Adsorption Properties and Effective Catalytic Performance

Arnon Khamkeaw^{1,2}, Tatdanai Asavamongkolkul¹, Tianpichet Perngyai¹,
Bunjerd Jongsomjit^{1,2} and Muenduen Phisalaphong^{1,*} 

¹ Bio-Circular-Green-economy Technology & Engineering Center, BCGeTEC, Department of Chemical Engineering, Faculty of Engineering, Chulalongkorn University, Bangkok 10330, Thailand; arnon.k1231@gmail.com (A.K.); tatdanai.asa@gmail.com (T.A.); tianpichet.p@hotmail.com (T.P.); bunjerd.j@chula.ac.th (B.J.)

² Center of Excellence on Catalyst and Catalytic Reaction Engineering, Department of Chemical Engineering, Faculty of Engineering, Chulalongkorn University, Bangkok 10330, Thailand

* Correspondence: muenduen.p@chula.ac.th; Tel.: +662-218-6875

Academic Editor: Dipendu Saha

Received: 6 August 2020; Accepted: 3 September 2020; Published: 5 September 2020



Abstract: The porous carbon (bacterial cellulose (BC)-activated carbon (AC)(BA)) prepared via two-step activation of bacterial nanocellulose by treatments with potassium hydroxide (KOH) and then phosphoric acid (H₃PO₄) solutions showed superior adsorption properties and effective performance as catalyst support. BC-AC(BA) had an open and interconnected multi-porous structure, consisting of micropores (0.23 cm³/g), mesopores (0.26 cm³/g), and macropores (4.40 cm³/g). The BET surface area and porosity were 833 m²/g and 91.2%, respectively. The methylene blue adsorption test demonstrated that BC-AC(BA) was superior in its mass transfer rate and adsorption capacities. Moreover, BC-AC(BA) modified by H₃PO₄ treatment showed a significant enhancement of catalytic performance for dehydration of ethanol. At the reaction temperature of 250–400 °C, 30P/BC-AC(BA) gave ethanol conversion at 88.4–100%, with ethylene selectivity of 82.6–100%, whereas, high selectivity for diethyl ether (DEE) at 75.2%, at ethanol conversion of 60.1%, was obtained at the reaction temperature of 200 °C.

Keywords: activated carbon; bacterial cellulose; catalyst; ethanol dehydration; adsorption

1. Introduction

Activated carbon (AC) is a carbonaceous material with high porosity, high surface area, high physical and chemical stability, high adsorptive activity, high mechanical strength, high thermal stability, and low cost [1]. These properties lead to a wide variety of industrial applications, such as an adsorbent in an adsorption process [2], catalyst or catalyst support in chemical reactions [3], material for removal of heavy metals from wastewater [4], and separator material in gas separation processes [5]. The production of AC has been prepared from many kinds of organic substances, such as agricultural by-products and residual wastes. Previously, our research works have presented that effective ACs can be prepared from bacterial cellulose (BC) [6,7]. BC has emerged as a renewable material in recent years. BC is a cellulosic biomaterial with the formula of (C₆H₁₀O₅)_n. It is produced by *Acetobacter xylinum* bacteria using sugars and other carbohydrate substrates as carbon sources. BC has a nanoporous structure formed by micro- and nanocellulose fibers with unique properties, including its high porosity, high degree of crystallinity, high surface area for adsorption, high tensile strength, high water-retention

capacity, low solubility, and resistance to organic solvents [8]. BC is of a high purity of cellulose because its structure does not contain lignin, hemicelluloses, or other complex carbohydrates. Because of these properties, BC should have great potential to be used as source material for highly efficient activated carbon. During the carbonization process, high amounts of oxygen-containing functional groups in cellulose tend to be eliminated as H_2O , CO_2 , and CO , resulting in BC-derived activated carbon with high porosity and high surface area [6,7]. BC-derived activated carbon (BC-AC) was used as an adsorbent for removing methylene blue (MB) from aqueous solutions [6] and was applied as green catalyst support for ethanol conversion to ethylene in ethanol dehydration reaction [7]. BC-AC showed high adsorption properties and effective performance as catalyst support. However, its structure with very small pore sizes could limit the mass transfer efficiency. The diffusion in small pores often results in a limitation of mass transfer, which could make the molecules of reactants and products difficult to diffuse in and out of the catalysis. In addition, the micro/mesoporous structure of BC-AC catalyst could lead to pore blockage by coke deposition, resulting in catalyst deactivation [9]. To overcome this mass transfer limitation, this study aimed to develop BC-AC with an improved porous structure, high porosity and high surface area.

From our previous works, BC-AC was synthesized by one-step chemical activation, using either potassium hydroxide (KOH) or phosphoric acid (H_3PO_4). By using KOH as an activating agent [10], the BC-AC showed high porosity with meso/macroporous structure, but it had low surface area. By using phosphoric acid (H_3PO_4) as an activating agent [6,7], the BC-AC exhibited a high surface area with micro/meso porous structure. The synthesis of highly porous AC from BC with an interconnected micro-, meso-, and macroporous structure was firstly introduced in this study, in which the two step chemical activations using both H_3PO_4 and KOH as activating agents were performed to improve the porous structure. The use of H_3PO_4 is intended to provide mesopores with high surface area, whereas the use of KOH aims to provide high porosity with large pore width. Therefore, by applying this two-step chemical activation, an interconnected micro-, meso-, and macroporous AC derived from BC with high adsorption rate combined with high adsorption capacity could be developed. The adsorptive and mass transfer performances of the altered ACs were investigated by MB adsorption. Then, ACs were modified by H_3PO_4 loading for improving surface acidity and further applied as a solid acid catalyst for the ethanol dehydration reaction.

2. Results and Discussion

2.1. Characterizations

2.1.1. SEM

ACs derived from BCs (BC-AC) were prepared by one-step and two-step chemical activation with H_3PO_4 (A) and/or KOH (B) as activating agent using an incipient wetness technique. The samples obtained from one-step activation are denoted as BC-AC(X), where X is the activating agent, i.e., BC-AC(A) refers to an AC derived from BC with H_3PO_4 (A) activation. The samples obtained from two-step activation are denoted as BC-AC(YZ), where Y is the first activating agent in first step activation, and Z is the second activating agent in second step activation, i.e., BC-AC(AB) refers to an AC derived from BC by using H_3PO_4 (A) as first activating agent in first step activation and KOH (B) as second activating agent in second step activation.

According to the XRD patterns of BC-ACs, all samples displayed only a diffraction peak at around 25° , indicating that all samples are amorphous materials composed of aromatic carbon sheets (Figure 1). Figure 2 shows the surface morphology and porous structure of BC-ACs. Before activating, the BC hydrogel has ultra-fine network structure consists of nano- and microfibers [11]. This structure is preserved even after being dried. After activating with strong acid and strong base at high temperature, the surface morphology of the BC has changed because the micropores, mesopores, and macropores were created in the structure resulting in the higher surface area. However, the raw form of BC that has nano- and microfibers network structure and high porosity is also inherited to the BC-ACs resulting in

the high porosity. Under one-step chemical activation, the obtained BC-AC(A) from the activation of BC with H_3PO_4 shows rough surfaces with mainly micropores and mesopores, whereas the obtained BC-AC(B) from the activation of BC with KOH was mainly composed of meso/macropores with large and deep cavities. Therefore, H_3PO_4 and KOH agents played different roles on the structure development of the BC-ACs. The using H_3PO_4 as an activating agent could lead to bond cleavage and formation of cross-linked structure. When the concentrated H_3PO_4 reacted with cellulose, the cellulose is depolymerized and linked to H_3PO_4 under the form of cellulose phosphate esters [12]. During the activation process, the oligomerized H_3PO_4 that become part of the carbon matrix transformed into P_2O_5 and water. The sublimation of P_2O_5 leads to the generation of pores; meanwhile, the evaporation of water molecules leads to the development of porosity [13]. On the other hand, KOH activation involves mainly fragmentation and solubilization of raw structure of precursor via a reduction reaction while leaving potassium-containing atoms within the carbon network. The potassium compound products can diffuse and intercalate into the carbon lamellae to induce the separation of layer and pore development [14]. This increases the net volume of the precursor and lowers its density. This may be associated with larger porous structure development that results in higher porosity. Under two-step chemical activation, BC-AC(AB), which was obtained from BC-AC(A) secondly chemical activated with KOH, presented more macropores, whereas the numbers of micropores and mesopores decreased due to the expansion of some micro/mesopores into macropores. The collapse of pore structure of BC-AC(AB) after the carbonization process at 500 °C was observed. On the other hand, BC-AC(BA) obtained from BC-AC(B) secondly chemical activated with H_3PO_4 presented micropores and mesopores restricted to surface of macropores. Therefore, a well-defined open and interconnected micro-, meso-, and macroporous structure can be created by two-step activation by KOH solution and followed by H_3PO_4 solution.

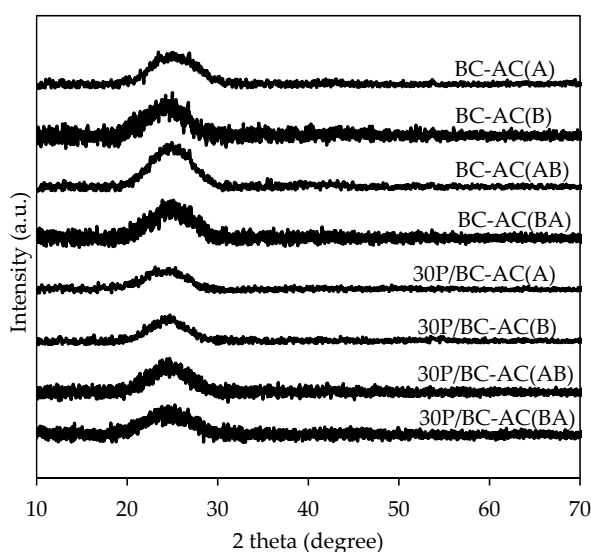


Figure 1. XRD patterns of bacterial cellulose-activated carbons (BC-ACs) and 30P/BC-ACs.

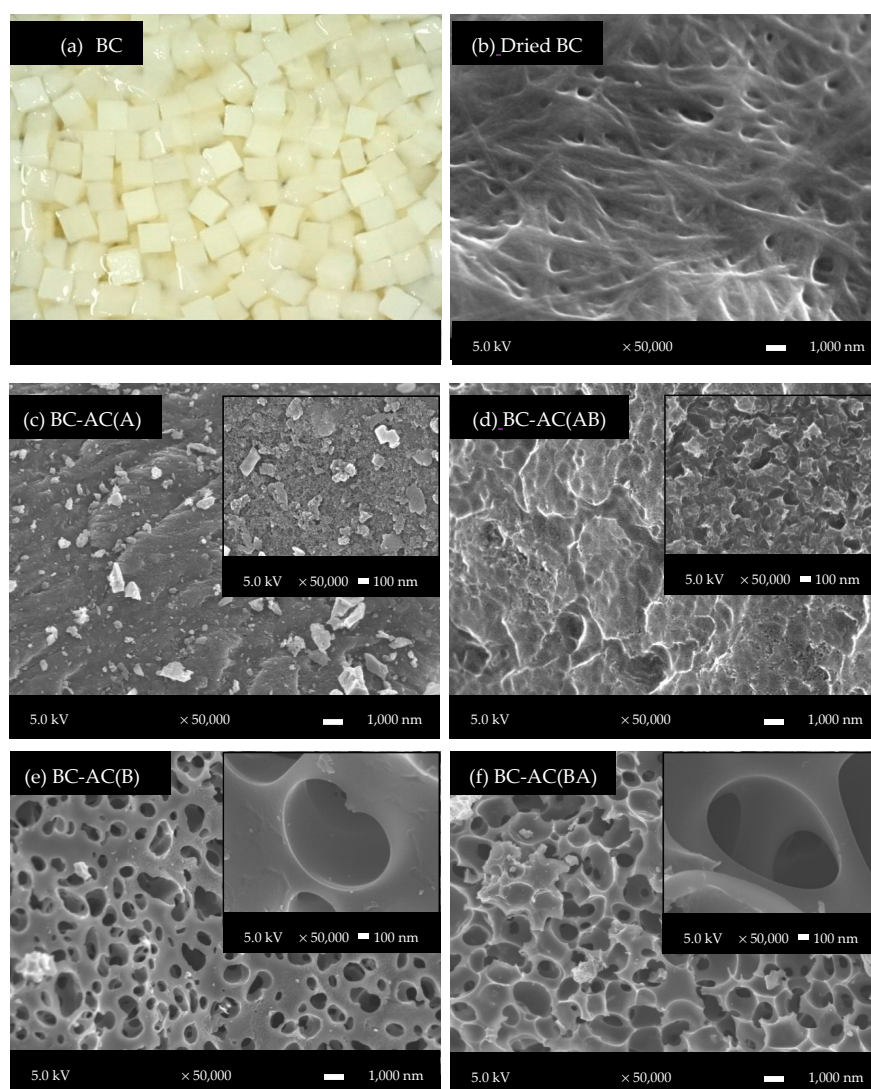


Figure 2. Images of (a) BC and SEM micrograph of surface morphology of (b) dried BC and (c–f) BC-ACs.

2.1.2. Pore Structure and Surface Area Analysis

The N_2 physisorption was used to determine micropore and mesopore characteristics (pore size diameter 0–50 nm). Meanwhile, the mercury porosimetry was used to determine macropore characteristics (pore size diameter 50–500,000 nm). Table 1 shows the surface area and pore volume of BC-ACs. BC-AC(A) exhibited high BET surface area of $1316 \text{ m}^2/\text{g}$, which was significantly higher than BC-AC(B). The pore-structure of BC-AC(A) has a porosity of 65.0%, consisted of micropores at volume of $0.17 \text{ cm}^3/\text{g}$ and mesopores at volume of $0.71 \text{ cm}^3/\text{g}$. BC-AC(A) exhibited lower macropore volume and less porosity than BC-AC(B). BC-AC(B) has a higher porosity of 79.7% and consisted of high macropores at volume of $3.3 \text{ cm}^3/\text{g}$. Owing to the effect of activating agents, H_3PO_4 produced AC with high surface area of micropores and mesopores [6], whereas KOH produced AC with macroporous structure and high porosity [10]. After the second chemical activation with KOH, the BET surface area and the micropore and mesopore volume of BC-AC(AB) decreased, whereas the macropore volume and porosity of BC-AC(AB) increased. Therefore, the macropores could be generated in-situ after the activation of BC-AC(A) with KOH. The results also demonstrate that, after the second activation of BC-AC(B) with H_3PO_4 , the BET surface area, micropore and mesopore volume, macropore volume, and porosity of BC-AC(BA) significantly increased as compared to BC-AC(B) due to the enlarged

macropores and the formation of micro/mesopores restricted to the surface of macropores during the carbonization process. The high macropore volume of 4.4 cm³/g and porosity of 91.2% were obtained.

Table 1. The surface area, pore volume, and porosity of BC-ACs.

| Activated Carbons | BET Surface Area ^a (m ² /g) | Pore Volume (cm ³ /g) | | | Average Pore Size Diameter (nm) | | Porosity ^b (%) |
|-------------------|---|----------------------------------|-------------------|--------------------|---------------------------------|--------------------|---------------------------|
| | | ^a Micro | ^a Meso | ^b Macro | ^a Micro-Meso | ^b Macro | |
| BC-AC(A) | 1316 | 0.17 | 0.71 | 1.00 | 2.4 | 54 | 65.0 |
| BC-AC(B) | 340 | 0.13 | 0.09 | 3.30 | 2.6 | 1730 | 79.7 |
| BC-AC(AB) | 551 | 0.15 | 0.19 | 1.60 | 2.7 | 265 | 71.3 |
| BC-AC(BA) | 833 | 0.23 | 0.26 | 4.40 | 2.5 | 2,704 | 91.2 |

^a Determination by N₂ physisorption. ^b Determination by mercury porosimetry.

N₂ adsorption-desorption isotherms are shown in Figure 3. The BC-AC(A) exhibited a complete hysteresis loop at the relative pressure ≥ 0.4 , whereas the BC-AC(AB) lacked closure of the hysteresis loop below a relative pressure of 0.4, which might be due to the expansion of a mesoporous to macroporous structure [15]. No hysteresis loops between the adsorption/desorption isotherms exist in BC-AC(B) and BC-AC(BA) due to the very high proportion of macropore volume in the porous structure [16]. According to International Union of Pure and Applied Chemistry (IUPAC) classification of physisorption isotherms [17], the isotherm of BC-AC(A) was type IV, which indicates a mesoporous structure, whereas the isotherms of the BC-AC(AB), BC-AC(B), and BC-AC(BA) were type II, which are associated with a macroporous structure.

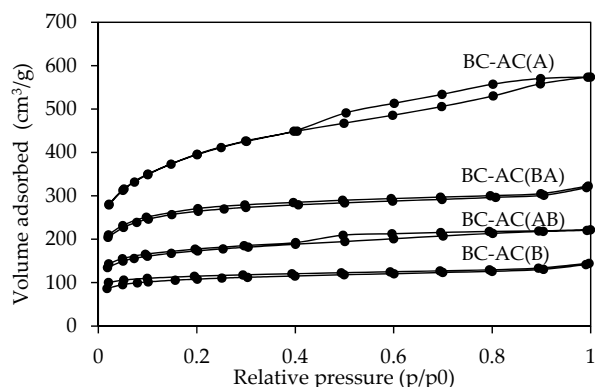


Figure 3. The N₂ adsorption-desorption isotherms of BC-ACs.

Figure 4 shows the pore size distribution of BC-ACs determined using N₂ physisorption and mercury porosimetry. BC-ACs show a pore size distribution range of micropores and mesopores at 1.2–15.5 nm (Figure 4a). BC-AC(A) has the highest surface area, followed by BC-AC(BA), BC-AC(AB), and BC-AC(B), respectively. The macropores were verified by the mercury porosimetry method, as shown in Figure 4b. BC-AC(B) and BC-AC(BA) had much larger macropore volumes than those of BC-AC(A) and BC-AC(AB). The result demonstrates that the two-step chemical activations can promote multiporous structures with high porosity. The surface area and porosity of BC-ACs were compared with AC derived from jackfruit leaf [18]. Jackfruit leaf is one of natural cellulose fiber sources (without nano structure). At the same activation temperature and activating agent, BC-ACs had significantly higher surface area and porosity. ACs derived from jackfruit leaf had a surface area of 67 and 44 m²/g by the activation with H₃PO₄ and KOH, respectively, with a porosity of 51 and 36%, respectively, which was relatively low as compared to ACs derived from BC (Table 1). This indicated that the raw nanostructure of BC can promote the high porosity in the porous structure of AC during the activation process.

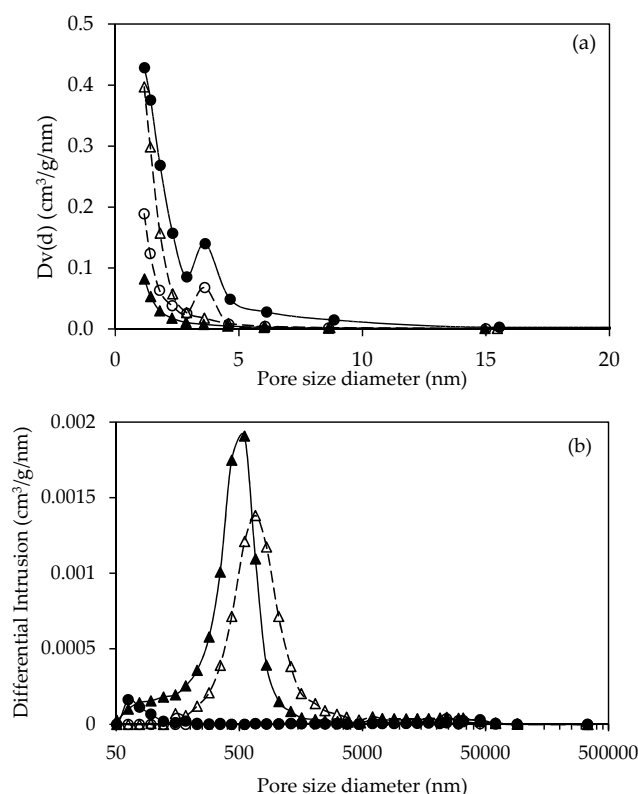


Figure 4. The pore size distribution of BC-AC(A) (●), BC-AC(B) (▲), BC-AC(AB) (○), and BC-AC(BA) (Δ) from N₂ physisorption (a) and mercury porosimetry (b).

2.1.3. Acidity

The surface acidity of BC-ACs was modified with H₃PO₄ treatment using the incipient wetness technique in order to further apply as solid acid catalysts in an ethanol dehydration reaction. According to a previous study [7], the optimal H₃PO₄ loading on BC-AC is 30 wt %. The solid catalysts of 30P/BC-ACs are BC-ACs loaded with 30 wt % H₃PO₄ (i.e., 30P/BC-AC(A) refers to BC-AC(A) loaded with 30 wt % of H₃PO₄).

The temperature-programmed desorption of ammonia (NH₃-TPD) was used to determine surface acidity and strength of acid sites of samples. The desorption temperature indicates the acid strength of the sites, with weaker sites desorbing at low temperatures (<250 °C) defined as weak acid sites, while those desorbing at high temperatures (250–500 °C) were defined as moderate to the strong acid sites [19]. Table 2 shows the summary of the number of the acid sites before and after modification of surface acidity with H₃PO₄ treatment. Before surface modification of BC-ACs, the amounts of weak acid sites and moderate to strong acid sites depend on the surface area of catalysts, listed in order from high to low, were as follows: BC-AC(A) > BC-AC(BA) > BC-AC(AB) > BC-AC(B). High surface area provides high amount of phosphate groups on the surface, which are formed on the carbon surface during the activation process of BC-ACs. The P-OH groups and phosphate ester and/or phenol groups correspond to weak acid sites, and the H-phosphate groups correspond to moderate to strong characters [20]. After the modification of BC-ACs surface acidity with 30% loading of H₃PO₄, the 30P/BC-ACs show higher numbers of weak acid sites and moderate to strong acid sites than BC-ACs. In a comparison between the amount weak acid site and moderate to strong acid sites, the BC-ACs and 30P/BC-ACs had higher amounts of weak acid sites than moderate to strong acid sites. Moreover, the H₃PO₄ modification enhanced the ratio of weak/moderate to strong from 1.9–2.0 to 2.8–3.9. It has been reported previously that the catalysts associated with a larger number of weak acid sites have good performance in ethanol dehydration because the ethanol conversion to ethylene occurs on weak acid sites, whereas the oligomerization and alcohol transformation to higher hydrocarbons

correspond to strong acid strength [21]. After loading of H_3PO_4 , the amounts of weak acid sites, listed in order from high to low, were as follows: 30P/BC-AC(A) > 30P/BC-AC(BA) > 30P/BC-AC(AB) > 30P/BC-AC(B).

Table 2. Acidity of BC-ACs and 30P/BC-ACs.

| Samples | Acid Sites ^a ($\mu\text{mol NH}_3/\text{g Catalyst}$) | | | |
|---------------|--|--------------------|-------|-------------------------|
| | Weak | Moderate to Strong | Total | Weak/Moderate to Strong |
| BC-AC(A) | 206 | 109 | 282 | 1.9 |
| BC-AC(B) | 94 | 49 | 143 | 1.9 |
| BC-AC(AB) | 110 | 54 | 164 | 2.0 |
| BC-AC(BA) | 130 | 68 | 198 | 1.9 |
| 30P/BC-AC(A) | 1141 | 294 | 1436 | 3.9 |
| 30P/BC-AC(B) | 528 | 173 | 701 | 3.1 |
| 30P/BC-AC(AB) | 609 | 209 | 818 | 2.9 |
| 30P/BC-AC(BA) | 837 | 299 | 1136 | 2.8 |

^a Quantities of acid sites of catalysts were determined using temperature-programmed desorption of ammonia (NH_3 -TPD) with Fityk program calculation.

2.1.4. FTIR

Figure 5 shows FTIR spectra of BC-ACs and 30P/BC-ACs. The broad band in the region of $3700\text{--}3200\text{ cm}^{-1}$ is attributed to O-H stretching vibration of hydroxyl group [6]. The band at approximately $\sim 1700\text{ cm}^{-1}$ is attributed to C=O stretching vibrations of ketones, aldehydes, lactones, or carboxyl groups [22]. The strong band at 1600 cm^{-1} is ascribed to the C-C stretching vibrations from aromatic rings. The broad band at approximately $\sim 1220\text{ cm}^{-1}$ may correspond to C-O stretching in acids, alcohols, phenols, ethers, and/or esters groups [22]. The aromatic character of the carbon is confirmed by the peaks at 880 cm^{-1} associated with aromatic C-H out-of-plane vibrations for different substituted benzene rings, which are evidence of the carbon [22]. The two bands at 980 and 500 cm^{-1} are assigned to the stretching vibrational mode of hydrogen-bonded P=O, to O-C stretching vibrational in P-O-C (aromatic) linkage, and to O=P-OH groups [23]. The presence of P-O and P-OH on the carbon surface can act as Brønsted acid sites, and they play an important role in the acidic character of the carbon catalysts prepared for ethanol dehydration [7]. After the modification of BC-ACs surface with H_3PO_4 treatment, the 30P/BC-ACs show higher phosphate group characteristics on the surface at two bands of 980 and 500 cm^{-1} , which is consistent with the surface acidity results.

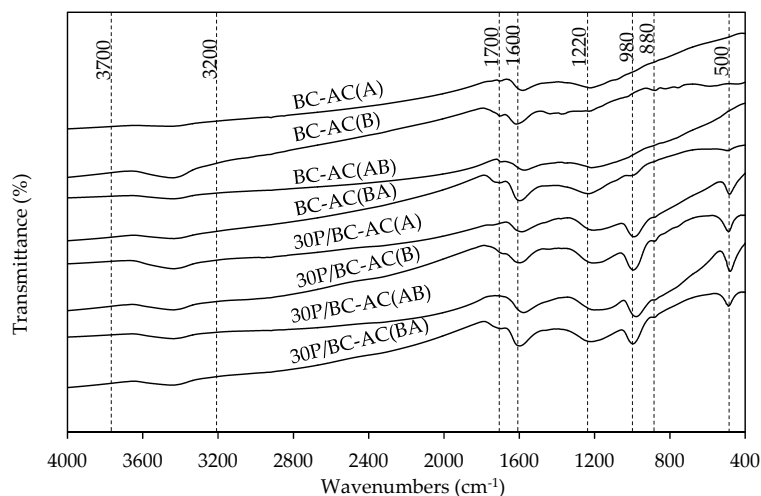


Figure 5. FT-IR patterns of BC-ACs and 30P/BC-ACs.

2.1.5. XPS

X-ray photoelectron spectroscopy (XPS) analyses were carried out in order to evaluate the surface element distribution and surface chemical structure of the samples. Figure 6a shows the wide range-scanning spectrum of BC-ACs and 30P/BC-ACs. The spectra of BC-ACs shows clearly C and O peaks, representing the major constituents of surface, while the spectra of 30P/BC-ACs shows major peaks of C, O and small peak of P. These results correspond to the results obtained from FTIR spectroscopy. After modification surface with H_3PO_4 , the 30P/BC-ACs show P group characteristics on the surface. Mass surface concentrations of BC-ACs and 30P/BC-ACs are shown in Table 3. The 30P/BC-ACs contained considerably higher amounts of P and O as compared to the BC-ACs. The amounts of P on 30P/BC-ACs surface were as follows: 30P/BC-AC(A) > 30P/BC-AC(BA) > 30P/BC-AC(AB) > 30P/BC-AC(B), which corresponded to the quantities of acid sites of 30P/BC-ACs as shown in Table 2. The small amount of Si was detected despite being a non-common constituent of AC derived from cellulose, which could be an inorganic impurity, sometimes detected from the energy dispersive spectrum of AC [24]. In order to describe the P groups bonded to a carbon site after the modification surface with H_3PO_4 , the XPS spectra of P 2p zone of 30P/BC-ACs was examined. The deconvolution of XPS spectra and the relative amount of phosphorus surface groups are shown in Figure 6b, and Table 4, respectively. The peak at around 135.7 eV is ascribed to P groups bonded to one C atom and three O atoms as in C–O–PO₃ and (C–O)₃PO [20]. The peak at around 134.8 eV is characteristic of C–P bonding as in C–PO₃ and C₂PO₂ groups [20]. The peak position slightly shifted from the maximum of the P 2p band to lower binding energy for 30P/BC-AC(B), 30P/BC-AC(AB), and 30P/BC-AC(BA) with an increase in the proportion of C–PO₃ and C₂PO₂ groups [25]. These acidic compounds were produced from the H_3PO_4 treatment. It was suggested that phosphates strongly bound to carbon lattice via C–O–P bonding; therefore, they are chemically and thermally stable [26]. This was again confirmed that the modification of surface acidity by the H_3PO_4 treatment effectively created Brønsted acid sites on carbon surface to be used as an effective acid catalyst for dehydration of ethanol.

Table 3. Mass surface concentration determined by XPS quantitative analysis of BC-ACs and 30P/BC-ACs.

| Samples | C (%) | O (%) | P (%) | N (%) | Si (%) |
|---------------|-------|-------|-------|-------|--------|
| BC-AC(A) | 74.3 | 20.7 | 3.1 | 1.9 | - |
| BC-AC(B) | 87.7 | 11.4 | - | - | 0.9 |
| BC-AC(AB) | 83.4 | 14.9 | - | 1.7 | - |
| BC-AC(BA) | 77.6 | 15.6 | 2.4 | 3.2 | 1.3 |
| 30P/BC-AC(A) | 24.5 | 52.1 | 22.5 | - | 0.9 |
| 30P/BC-AC(B) | 63.1 | 27.2 | 6.0 | 1.4 | 2.4 |
| 30P/BC-AC(AB) | 55.9 | 30.5 | 11.5 | - | 2.2 |
| 30P/BC-AC(BA) | 48.6 | 37.0 | 12.6 | - | 1.8 |

Table 4. Relative amount of phosphorus surface groups obtained from deconvolution of P 2p zone of XPS spectra of 30P/BC-ACs.

| Samples | C–O–PO ₃ and (C–O) ₃ PO (%) | C–PO ₃ and C ₂ PO ₂ (%) |
|---------------|---|--|
| 30P/BC-AC(A) | 33.9 | 66.1 |
| 30P/BC-AC(B) | 24.1 | 75.9 |
| 30P/BC-AC(AB) | 30.3 | 69.7 |
| 30P/BC-AC(BA) | 38.9 | 61.1 |

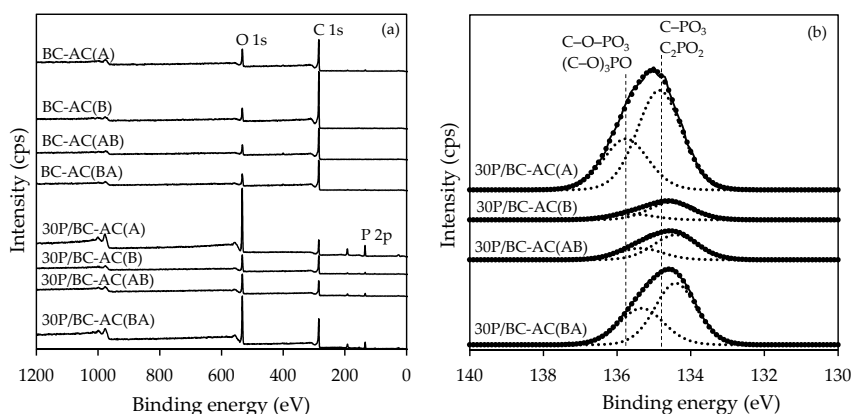


Figure 6. XPS wide scan spectra of all samples (a) and deconvolution of XPS spectra P 2p zone of 30P/BC-ACs (b).

2.2. Mass Transfer and Adsorption Capacity

To understand the diffusion in the porous structure of BC-ACs, the mass transfer performance of BC-ACs was studied in the adsorption of MB at the high initial MB concentration of 600 mg/L. Figure 7 shows the experimental kinetic data of all samples. A rapid initial rate of adsorption during 0–60 min was observed, which is likely due to the high MB concentration gradient between solution and adsorbents, creating fast transfer of solute ions to the surface of the adsorbents, and also the availability of the specific surface area of adsorbent sites [27]. BC-AC(BA) shows the best mass transfer performance with fastest adsorption rate in the adsorption of MB compared with BC-AC(A), BC-AC(AB), and BC-AC(B). Because BC-AC(BA) had the highest porosity with an open pore network structure, consisting of micro-, meso-, and macropores, it facilitated the diffusion of MB molecules in porous structure [28], resulting in the fastest mass transfer rate. The molecules of MB could more easily diffuse into the porous structure of BC-AC(BA). Adsorption equilibrium was reached after approximately 60 min for BC-AC(BA), ≈ 90 min for BC-AC(B), ≈ 120 min for BC-AC(AB), and ≈ 180 min for BC-AC(A). The faster adsorption rate was due to the higher macropore volume and higher porosity, which promoted the mass transfer of MB from the bulk solution into the interior of the adsorbents. Moreover, BC-AC(BA) had the highest adsorption capacity, with a maximum value of 593.4 mg/g. Although the BC-AC(A) had a larger surface area than BC-AC(BA), the structure with smaller pore sizes and lower porosity could limit the mass transfer efficiency, especially for the diffusion into the interior of BC-AC(A), leading to less adsorption capacity as compared to BC-AC(BA).

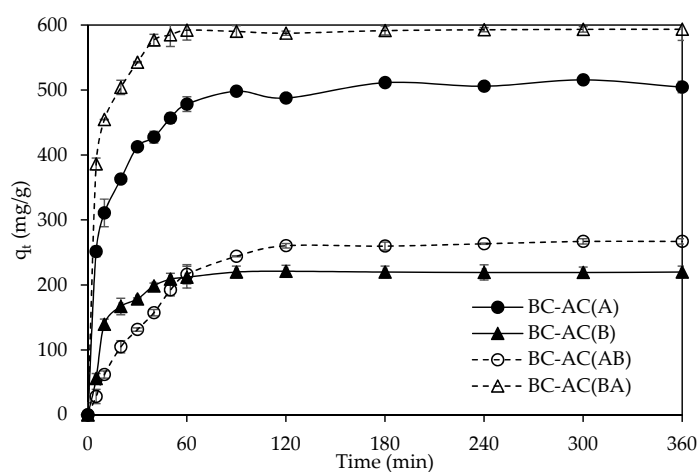


Figure 7. The adsorption kinetics of BC-AC(A) (●), BC-AC(B) (▲), BC-AC(AB) (○), and BC-AC(BA) (Δ) from methylene blue (MB) adsorption at initial concentration of 600 mg/L.

2.3. Catalytic Ethanol Dehydration Performance

Figure 8a presents the ethanol conversion of 30P/BC-AC catalysts. Similar effects related to reaction temperature and acidity of catalyst on the ethanol conversion have been previously reported [29]. The ethanol conversion of all 30P/BC-AC catalysts increased with increased reaction temperature from 200 °C to 400 °C because the ethanol dehydration reaction is an endothermic reaction that favors high temperature condition for the conversion of ethanol to ethylene [7]. The high conversion of ethanol at 100% was obtained by using 30P/BC-AC(BA) and 30P/BC-AC(A) at a reaction temperature of 350–400 °C. At lower reaction temperatures (below 350 °C), 30P/BC-AC(BA) shows a higher conversion of ethanol than the other catalysts. Overall, 30P/BC-AC(BA) gave the highest catalytic activity, i.e., 60.1% of ethanol conversion at reaction temperature of 200 °C, and 88.4–100% of ethanol conversion at reaction temperature of 250–400 °C. Although 30P/BC-AC(A) had more weak acid sites as compared to 30P/BC-BC500(BA), it was shown that, with the higher macropore volume and porosity, the enhanced mass transfer inside the catalyst could be promoted, resulting in effective overall catalytic activities of 30P/BC-BC500(BA). Owing to suitable porous structure, the reactants can easily diffuse into the catalyst pores and are converted to products at active sites [30], and the obtained products can easily diffuse out of the catalyst. The interconnected micro-, meso-, and macroporous structure gives the catalyst with a high number of active sites and high internal diffusion.

All 30P/BC-AC catalysts show the highest ethylene selectivity at the reaction temperature of 400 °C (Figure 8b), at which the ethylene selectivity of 100%, 100%, 99.1%, and 89.0% were obtained from BC-AC(BA), BC-AC(A), BC-AC(B), and BC-AC(AB), respectively. However, at lower reaction temperatures below 400 °C, the ethylene yield obtained with 30P/BC-AC(BA) was considerably higher than those obtained by using 30P/BC-AC(A), 30P/BC-AC(B), and 30P/BC-AC(AB). Overall, the order of catalytic performance from high to low was as follows: 30P/BC-AC(BA) > 30P/BC-AC(A) > 30P/BC-AC(B) > 30P/BC-AC(AB). The 30P/BC-AC(BA) gave the selectivity of ethylene of 82.6–99.4% at the reaction temperature range of 250–350 °C. The selectivity of ethylene of all 30P/BC-AC catalysts decreased with decreased reaction temperature due to the more conversion of ethanol into DEE and acetaldehyde. At 200 °C, the selectivity for DEE (Figure 8c) was as follows: 61.5% for 30P/BC-AC(B), 68.4% for 30P/BC-AC(A), and 75.2% for 30P/BC-AC(BA), whereas the selectivity of acetaldehyde as the dominant product from 30P/BC-AC(AB) was 100% at 200 °C (Figure 8d). However, because of the low ethanol conversion of 30P/BC-AC(AB) at 200 °C, the acetaldehyde yields were quite low (21.0%).

Table 5 shows the yield of ethylene, diethyl ether (DEE), and acetaldehyde (MeCHO) from ethanol dehydration at 200, 250, 300, and 400 °C. Among all 30P/BC-AC catalysts, the 30P/BC-AC(BA) provided the highest ethylene yield of 73.0–100.0% at the reaction temperature range of 250–400 °C, and the highest DEE yield of 45.2% at the reaction temperature of 200 °C. Therefore, the 30P/BC-AC(BA) catalyst is considered to be the most promising catalyst for ethanol dehydration for both ethylene production at 300–400 °C and DEE production at 200 °C.

Table 5. Yield of ethylene, diethyl ether (DEE), and acetaldehyde (MeCHO) from ethanol dehydration at 200, 250, 300, and 400 °C.

| Catalysts | 200 °C | | | 250 °C | | | 300 °C | | | 400 °C | | |
|---------------|----------|------|-------|----------|------|-------|----------|-----|-------|----------|-----|-------|
| | Ethylene | DEE | MeCHO | Ethylene | DEE | MeCHO | Ethylene | DEE | MeCHO | Ethylene | DEE | MeCHO |
| 30P/BC-AC(A) | 7.1 | 34.5 | 2.5 | 24.9 | 32.1 | 4.7 | 90.5 | 6.8 | 1.1 | 100.0 | 0.0 | 0.0 |
| 30P/BC-AC(B) | 0.7 | 16.4 | 1.0 | 19.0 | 34.5 | 8.6 | 85.9 | 2.2 | 2.8 | 94.8 | 0.3 | 0.6 |
| 30P/BC-AC(AB) | 0.0 | 0.0 | 21.0 | 3.3 | 7.9 | 18.8 | 24.1 | 7.9 | 11.2 | 61.3 | 0.7 | 6.8 |
| 30P/BC-AC(BA) | 9.0 | 45.2 | 1.5 | 73.0 | 13.5 | 1.9 | 95.8 | 2.6 | 0.8 | 100.0 | 0.0 | 0.5 |

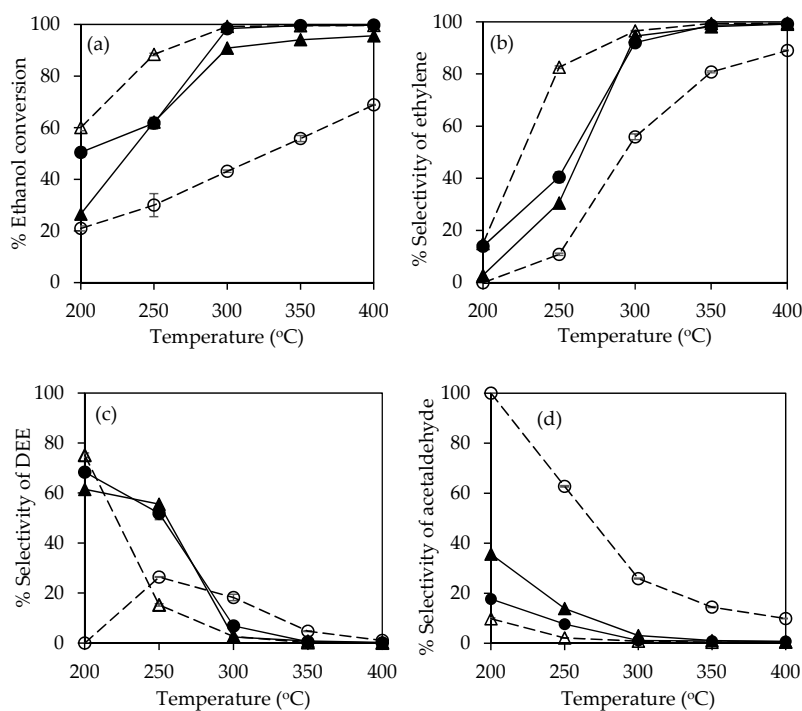


Figure 8. Ethanol conversion (a), selectivity of ethylene (b), selectivity of diethyl ether (DEE) (c), and selectivity of acetaldehyde (d) in ethanol dehydration at reaction temperatures of 200–400 °C using the BC-AC(A) (●), BC-AC(B) (▲), BC-AC(AB) (○), and BC-AC(BA) (Δ) catalysts.

2.4. Stability Test

Because of its excellent catalytic performance, 30P/BC-AC(BA) was selected for the study of catalyst stability with a time-on-stream of 12 h. Figure 9 shows the ethanol conversions during the 12-h stability tests at reaction temperatures of 200 and 400 °C. At the low reaction temperature of 200 °C, the ethanol conversion and selectivity for DEE were quite stable at around 51.2–60.6% and 73.3–79.9%, respectively. At the high reaction temperature of 400 °C, the ethanol conversion was constant at 100%, with an ethylene selectivity of 100% during the 12-h stability test. These results indicate that the 30P/BC-AC(BA) catalyst has a very high catalytic activity and high stability in ethanol dehydration for the production of ethylene and DEE. In addition, 30P/BC-AC(BA) catalyst can be considered as a green catalyst because it is derived from bacterial cellulose and it is eco-friendly.

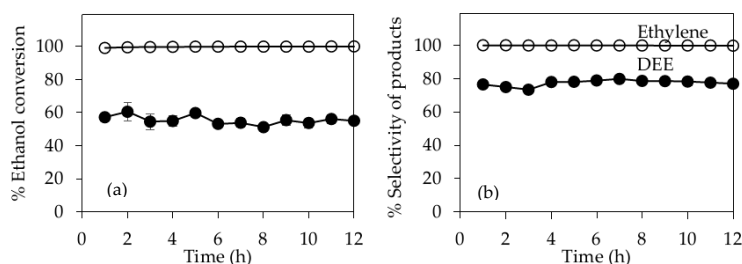


Figure 9. Stability test with a time-on-stream (TOS) for 30P/BC-AC(BA) catalyst at reaction temperature of 200 (●) and 400 °C (○): (a) Ethanol conversion, (b) Selectivity of products.

The performances of 30P/BC-AC(BA) and different catalysts using H_3PO_4 modification [31–33], different carbon-based catalysts [7,9,19,34], and other catalysts [35], with respect to ethanol conversion, ethylene selectivity, and DEE selectivity were compared as shown in Table 6. It has been demonstrated that 30P/BC-AC(BA) has excellent catalytic performance.

Table 6. Comparison of catalysts for ethanol dehydration and their catalytic ability.

| Catalysts | Reaction Temperature (°C) | Ethanol Conversion (%) | Ethylene Selectivity (%) | DEE Selectivity (%) | References |
|-----------------------------------|---------------------------|------------------------|--------------------------|---------------------|------------|
| 30P/BC-AC(BA) | 200–400 | 60.1–100 | 15.0–100 | 75.2–0.0 | This work |
| 30P/BC-AC500 | 200–400 | 50.5–100 | 13.9–100 | 68.4–0.0 | [7] |
| 20HP-ZSM-5 | 250–400 | 25.0–99.0 | 3.0–99.0 | 96–0.0 | [31] |
| 5P/Al ₂ O ₃ | 200–400 | 9.1–86.1 | 0.0–94.0 | 100–6.0 | [32] |
| 30PA-CeO ₂ | 400–500 | 16.0–59.7 | 96.1–99.2 | 0.2–0.1 | [33] |
| 25Al/BC-FD | 200–400 | 41.3–65.7 | 1.1–43.3 | 40.0–43.3 | [19] |
| HA2-800 | 200–350 | 2.0–100 | 34.0–100 | 65.0–0 | [9] |
| AC_H420 | 400 | 39.1 | 69.4 | 29.9 | [34] |
| SiO ₂ | 200–400 | 0.0–8.6 | 0.0–48.8 | 0.0–31.8 | [35] |
| ZrO ₂ | 200–400 | 0.0–100.0 | 0.0–75.4 | 0.0–1.5 | [35] |
| TiO ₂ | 200–400 | 0.6–100.0 | 0.0–29.7 | 83.8–0.0 | [35] |

3. Materials and Methods

3.1. Materials

BC was synthesized by *A. xylinum* strain AGR 60. BC hydrogel was treated with 1% *w/v* NaOH for 24 h to remove bacterial cells, and then it was rinsed with deionized (DI) water until pH was 7.0 and was dried at 110 °C for 24 h.

3.2. Activated Carbon and Catalyst Preparation

BC-ACs were prepared by chemical activation with H₃PO₄ and/or KOH as activating agent using an incipient wetness technique. For one-step activation in the synthesis of BC-AC(A), dried BCs (size ≈ 1 × 1 × 0.1 cm³) were soaked with 85 wt % H₃PO₄ at 30 °C for 24 h, whereas, in the synthesis of BC-AC(B), dried BCs were soaked with 12 M of KOH at 30 °C for 24 h. After that, both impregnated BCs were dried at 110 °C for 24 h in a general electric oven (SNOL 67/350 LSP01, SNOL, Utena, Lithuania). The dried products were then carbonized at 500 °C in a muffle furnace (CWF 1100, Carbolite, Hope Valley, UK) (without any gas purging) for 1 h before cooling. For the two-step activation, the obtained BC-AC(A) and BC-AC(B) from the one-step activation were secondly chemical activated. For BC-AC(AB) synthesis, BC-AC(A) was secondly soaked with 12 M of KOH. For the BC-AC(BA) synthesis, BC-AC(B) was secondly soaked with 85 wt % of H₃PO₄. Then, they were dried and carbonized under similar conditions as previously described.

In order to be used as solid acid catalysts in ethanol dehydration reaction, the surface acidity of BC-AC(A), BC-AC(B), BC-AC(AB), and BC-AC(BA) was further modified by H₃PO₄ treatment. BC-ACs were impregnated with H₃PO₄ solution (30 wt % H₃PO₄) by the incipient wetness method. The solution of H₃PO₄ was dropped slowly onto 0.1 g of BC-ACs, and the BC-AC catalysts were then dehydrated in a general electric oven at 110 °C for 24 h.

3.3. Characterizations

The surface area, porosity and micro/meso pore size distribution of samples were determined by nitrogen (N₂) physisorption-desorption using a micromeritics chemisorb 2750 pulse (Micromeritics, Norcross, GA, USA). The macropore volume and macropore size distributions were determined at pressure range of 0.1–61,000 psia by mercury porosimetry (AutoPore V 9600 version 1.03, Micromeritics, Norcross, GA, USA). The morphology of samples was determined by field emission scanning electron microscope (FESEM) (Model of JSM-7610F, JEOL, Oxford, MS, USA). The surface chemistry of samples was analyzed by the Fourier transform infrared (FTIR) spectroscopy (Nicolet 6700 FTIR spectrometer, Thermo Scientific, Waltham, MA, USA) and X-ray photoelectron spectrometer (XPS) (Axis Ultra DLD, Kratos Analytical, Manchester, UK). The acid properties of samples were investigated by the temperature-programmed desorption of ammonia (NH₃-TPD) (Chemisorb2750 pulse, Micromeritics,

Norcross, GA, USA). The methodologies used for the characterizations were previously reported in detail elsewhere [6,7].

3.4. Mass Transfer and Adsorption Capacity

The performances of mass transfer and adsorption of BC-ACs were evaluated for the removal of MB from aqueous solution at initial MB concentration of 600 mg/L. The initial pH of MB solution was adjusted to pH 7.0 by adding 0.1 M NaOH. BC-ACs (0.02 g) were added into the MB solution (40 mL) in a 100 mL Erlenmeyer flask. The adsorption experiment was conducted at 30 °C and 125 rpm using an incubator shaker (Innova 4330, New Brunswick Scientific, Edison, NJ, USA). For the kinetics and equilibrium study of MB adsorption, the solution of 0.1 mL of each flask was taken every 10 min for 1 h and every 30 min for 2 h. The solution samples were filtered passed through the filter paper. The concentrations of MB in the solutions were analyzed by a UV-visible spectrophotometer (UV-2450, Shimadzu, Japan) at a wavelength of 664 nm. A calibration curve was used to relate the optical density (OD) measurements to MB concentrations in the solutions. The amount of MB adsorbed per gram of adsorbent at any given time (q_t , mg/g) was calculated by the following Equation (1):

$$q_t = \frac{(C_0 - C_t)V}{W} \quad (1)$$

where C_0 and C_t (mg/L) are the initial concentration and the concentration of the MB solution at any time, t , respectively. V (L) is the volume of the solution, and (W) g is the weight of the adsorbent used.

3.5. Catalytic Ethanol Dehydration Reaction and Catalytic Stability of Catalysts

The ethanol dehydration reaction has been carried out under atmospheric pressure in a fixed-bed continuous flow micro-reactor using 0.1 g of catalyst at the temperature in the range of 200 to 400 °C. For catalytic stability test, the catalyst that provided the highest catalytic ethanol dehydration was selected to investigate its stability for ethanol dehydration reaction as a function of time on stream (TOS) at the reaction temperature of 200 °C and 400 °C for 12 h. The processes were previously reported in detail elsewhere [7]. The ethanol conversion, selectivity and yield were calculated by the following formulas:

$$\text{Ethanol conversion (\%)} = \frac{(\text{moles of ethanol in feed} - \text{moles of ethanol in product})}{\text{moles of ethanol in feed}} \times 100 \quad (2)$$

$$\text{Selectivity (\%)} = \frac{\text{moles of desired product formed}}{\text{moles of total product formed}} \times 100 \quad (3)$$

$$\text{Yield (\%)} = \frac{\text{Ethanol conversion} \times \text{Selectivity}}{100} \quad (4)$$

4. Conclusions

BC was used as a carbon source for AC preparation due to its highly interconnected porous structure. A modified activation technique by two-step chemical activation was proposed. BC-AC(BA), which was prepared by the KOH activation, followed by the H_3PO_4 activation at a carbonization temperature of 500 °C showed the superior absorption performance. BC-AC(BA) has an interconnected multi-porous structure, composed of micropores ($0.23 \text{ cm}^3/\text{g}$), mesopores ($0.26 \text{ cm}^3/\text{g}$), and macropores ($4.40 \text{ cm}^3/\text{g}$) with porosity of 91.2% and BET surface area of $833 \text{ m}^2/\text{g}$. According to the improved porous structure, the mass diffusion in the particle was enhanced, resulting in a higher absorption rate. The adsorption capacity was also increased to 593.4 mg of MB/g. The catalyst of 30P/BC-AC(BA) was shown to be an efficient catalyst for the dehydration of ethanol to ethylene and DEE. Ethylene selectivity of 82.6–100% and ethanol conversion of 88.4–100% were obtained by using 30P/BC-AC(BA) at a reaction temperature range of 250–400 °C, whereas DEE selectivity of 75.2% and ethanol conversion

of 60.1% were obtained at the reaction temperature of 200 °C. Under a 12-h stability test, it was indicated that 30P/BC-AC(BA) was a very effective and selective catalyst with high stability in ethanol dehydration for the production of ethylene at 400 °C and the production of DEE at 200 °C.

Author Contributions: Conceptualization, M.P. and A.K.; methodology, M.P. and A.K.; validation, M.P. and A.K.; formal analysis, A.K., T.A., and T.P.; investigation, M.P., B.J., A.K., T.A., and T.P.; resources, M.P. and B.J.; data curation, A.K.; writing—original draft preparation, A.K.; writing—review and editing, M.P.; supervision, M.P.; project administration, M.P.; funding acquisition, M.P., B.J., and A.K. All authors have read and agreed to the published version of the manuscript.

Funding: This research was funded by Ratchadapisek Somphot Fund for Postdoctoral Fellowship, Chulalongkorn University and the International Research Network Program, Thailand Science Research and Innovation (IRN62W0001).

Acknowledgments: This research is supported by Ratchadapisek Somphot Fund for Postdoctoral Fellowship, Chulalongkorn University. The authors also would like to thank the International Research Network Program, Thailand Science Research and Innovation (IRN62W0001). for supporting this research.

Conflicts of Interest: The authors declare no conflict of interest.

References

1. Sharghi, H.; Aberi, M.; Doroodmand, M.M. Reusable Cobalt(III)-Salen Complex Supported on Activated Carbon as an Efficient Heterogeneous Catalyst for Synthesis of 2-Arylbenzimidazole Derivatives. *Adv. Synth. Catal.* **2008**, *350*, 2380–2390. [[CrossRef](#)]
2. Siriwardane, R.V.; Shen, M.-S.; Fisher, E.P.; Poston, J.A. Adsorption of CO₂ on Molecular Sieves and Activated Carbon. *Energy Fuels* **2001**, *15*, 279–284. [[CrossRef](#)]
3. Wu, X.; Zhu, F.; Qi, J.; Zhao, L. Biodiesel Production from Sewage Sludge by Using Alkali Catalyst Catalyze. *Procedia Environ. Sci.* **2016**, *31*, 26–30. [[CrossRef](#)]
4. Kadirvelu, K. Removal of heavy metals from industrial wastewaters by adsorption onto activated carbon prepared from an agricultural solid waste. *Bioresour. Technol.* **2001**, *76*, 63–65. [[CrossRef](#)]
5. Sircar, S.; Golden, T.; Rao, M. Activated carbon for gas separation and storage. *Carbon* **1996**, *34*, 1–12. [[CrossRef](#)]
6. Khamkeaw, A.; Jongsomjit, B.; Robison, J.; Phisalaphong, M. Activated carbon from bacterial cellulose as an effective adsorbent for removing dye from aqueous solution. *Sep. Sci. Technol.* **2018**, *54*, 2180–2193. [[CrossRef](#)]
7. Khamkeaw, A.; Phanthang, L.; Jongsomjit, B.; Phisalaphong, M.; Phathang, L. Activated carbon derived from bacterial cellulose and its use as catalyst support for ethanol conversion to ethylene. *Catal. Commun.* **2019**, *129*, 105750. [[CrossRef](#)]
8. Taokaew, S.; Seetabhawang, S.; Siripong, P.; Phisalaphong, M. Biosynthesis and Characterization of Nanocellulose-Gelatin Films. *Materials* **2013**, *6*, 782–794. [[CrossRef](#)]
9. Bedia, J.; Barrionuevo, R.; Rodríguez-Mirasol, J.; Cordero, T. Ethanol dehydration to ethylene on acid carbon catalysts. *Appl. Catal. B Environ.* **2011**, *103*, 302–310. [[CrossRef](#)]
10. Boongate, C.; Phisalaphong, M. Activated carbons from bacterial cellulose by chemical activation with potassium hydroxide. In Proceedings of the 2015 International Conference on Science and Technology (TICST), Pathum Thani, Thailand, 4–6 November 2015; pp. 144–147. [[CrossRef](#)]
11. Kamiń, K.; Jarosz, M.; Grudzień, J.; Pawlik, J.; Zastawnik, F.; Pandyr, P.; Kołodziejczyk, A.M. Hydrogel bacterial cellulose: A path to improved materials for new eco-friendly textiles. *Cellulose* **2020**, *27*, 5353–5365. [[CrossRef](#)]
12. Kokol, V.; Božič, M.; Vogrinčič, R.; Mathew, A.P. Characterisation and properties of homo- and heterogeneously phosphorylated nanocellulose. *Carbohydr. Polym.* **2015**, *125*, 301–313. [[CrossRef](#)] [[PubMed](#)]
13. Shi, Y.; Liu, G.; Wang, L.; Zhang, H. Activated carbons derived from hydrothermal impregnation of sucrose with phosphoric acid: Remarkable adsorbents for sulfamethoxazole removal. *RSC Adv.* **2019**, *9*, 17841–17851. [[CrossRef](#)]
14. Villota, S.M.; Lei, H.; Villota, E.; Qian, M.; Lavarias, J.; Taylan, V.; Agulto, I.; Mateo, W.; Valentin, M.; Denson, M. Microwave-Assisted Activation of Waste Cocoa Pod Husk by H₃PO₄ and KOH—Comparative Insight into Textural Properties and Pore Development. *ACS Omega* **2019**, *4*, 7088–7095. [[CrossRef](#)]

15. Cai, Y.; Liu, D.; Pan, Z.; Yao, Y.; Li, J.; Qiu, Y. Pore structure and its impact on CH₄ adsorption capacity and flow capability of bituminous and subbituminous coals from Northeast China. *Fuel* **2013**, *103*, 258–268. [CrossRef]
16. Jiang, H.; Cheng, Y.; Yuan, L. A Langmuir-like desorption model for reflecting the inhomogeneous pore structure of coal and its experimental verification. *RSC Adv.* **2015**, *5*, 2434–2440. [CrossRef]
17. Sing, K.S.W. Reporting Physisorption Data for Gas/Solid Systems with Special Reference to the Determination of Surface Area and Porosity. *Pure Appl. Chem.* **1985**, *57*, 603–619. [CrossRef]
18. Thomas, M.; Patel, S.P.; Patel, A.V.; Pate, J.V. A comparative study on the efficiency of KOH and H₃PO₄ impregnated jackfruit leaf based carbon as adsorbent for removal of Cr (VI) from its aqueous solution. *Int. J. Eng. Trends Technol.* **2017**, *45*, 176–182. [CrossRef]
19. Abdulwahab, M.I.; Khamkeaw, A.; Jongsomjit, B.; Phisalaphong, M. Bacterial Cellulose Supported Alumina Catalyst for Ethanol Dehydration. *Catal. Lett.* **2017**, *147*, 2462–2472. [CrossRef]
20. Bedia, J.; Ruiz-Rosas, R.; Rodríguez-Mirasol, J.; Cordero, T.; Bedia, J. Kinetic study of the decomposition of 2-butanol on carbon-based acid catalyst. *AIChE J.* **2009**, *56*, 1557–1568. [CrossRef]
21. Wannaborworn, M.; Praserttham, P.; Jongsomjit, B. A Comparative Study of Solvothermal and Sol-Gel-Derived Nanocrystalline Alumina Catalysts for Ethanol Dehydration. *J. Nanomater.* **2015**, *2015*, 1–11. [CrossRef]
22. Yakout, S.M.; El-Deen, G.S. Characterization of activated carbon prepared by phosphoric acid activation of olive stones. *Arab. J. Chem.* **2016**, *9*, S1155–S1162. [CrossRef]
23. Yorgun, S.; Yıldız, D. Preparation and characterization of activated carbons from Paulownia wood by chemical activation with H₃PO₄. *J. Taiwan Inst. Chem. Eng.* **2015**, *53*, 122–131. [CrossRef]
24. Gao, B. Acidified Activated Carbon with Enhanced Electrochemical Performance for Supercapacitors. *Int. J. Electrochem. Sci.* **2017**, *12*, 116–127. [CrossRef]
25. Rosas, J.M.; Bedia, J.; Rodríguez-Mirasol, J.; Cordero, T. Preparation of Hemp-Derived Activated Carbon Monoliths. Adsorption of Water Vapor. *Ind. Eng. Chem. Res.* **2008**, *47*, 1288–1296. [CrossRef]
26. Puziy, A.; Poddubnaya, O.; Ziatdinov, A. On the chemical structure of phosphorus compounds in phosphoric acid-activated carbon. *Appl. Surf. Sci.* **2006**, *252*, 8036–8038. [CrossRef]
27. Aysan, H.; Edebali, S.; Ozdemir, C.; Karakaya, M.C.; Karakaya, N. Use of chabazite, a naturally abundant zeolite, for the investigation of the adsorption kinetics and mechanism of methylene blue dye. *Microporous Mesoporous Mater.* **2016**, *235*, 78–86. [CrossRef]
28. Chen, B.; Yang, Z.; Ma, G.; Kong, D.; Xiong, W.; Wang, J.; Zhu, Y.; Xia, Y. Heteroatom-doped porous carbons with enhanced carbon dioxide uptake and excellent methylene blue adsorption capacities. *Microporous Mesoporous Mater.* **2018**, *257*, 1–8. [CrossRef]
29. Chen, G.; Li, S.; Jiao, F.; Yuan, Q. Catalytic dehydration of bioethanol to ethylene over TiO₂/γ-Al₂O₃ catalysts in microchannel reactors. *Catal. Today* **2007**, *125*, 111–119. [CrossRef]
30. Martins, L.; Cardoso, D.; Hammer, P.; Garetto, T.; Pulcinelli, S.H.; Santilli, C.V. Efficiency of ethanol conversion induced by controlled modification of pore structure and acidic properties of alumina catalysts. *Appl. Catal. A Gen.* **2011**, *398*, 59–65. [CrossRef]
31. Ramesh, K.; Hui, L.M.; Han, Y.; Borgna, A. Structure and reactivity of phosphorous modified H-ZSM-5 catalysts for ethanol dehydration. *Catal. Commun.* **2009**, *10*, 567–571. [CrossRef]
32. Limlamthong, M.; Chitpong, N.; Jongsomjit, B. Influence of Phosphoric Acid Modification on Catalytic Properties of γ-χ Al₂O₃ Catalysts for Dehydration of Ethanol to Diethyl Ether. *Bull. Chem. React. Eng. Catal.* **2019**, *14*, 1–8. [CrossRef]
33. Etilena, P.; Pendehidratan, D.; Dangan, E.; Serium, M. Production of ethylene from ethanol dehydration over H₃PO₄-modified cerium oxide catalysts. *Malaysian J. Anal. Sci.* **2018**, *21*, 839–848. [CrossRef]
34. Chaichana, E.; Wiwatthanodom, W.; Jongsomjit, B. Carbon-Based Catalyst from Pyrolysis of Waste Tire for Catalytic Ethanol Dehydration to Ethylene and Diethyl Ether. *Int. J. Chem. Eng.* **2019**, *2019*, 1–10. [CrossRef]
35. Phung, T.K.; Hernández, L.P.; Busca, G. Conversion of ethanol over transition metal oxide catalysts: Effect of tungsta addition on catalytic behaviour of titania and zirconia. *Appl. Catal. A Gen.* **2015**, *489*, 180–187. [CrossRef]

Sample Availability: Not available.



© 2020 by the authors. Licensee MDPI, Basel, Switzerland. This article is an open access article distributed under the terms and conditions of the Creative Commons Attribution (CC BY) license (<http://creativecommons.org/licenses/by/4.0/>).